Chapter 11
Evaluation of the HRRT - Results

放射線医学総合研究所
脳機能イメージング研究開発推進室
生駒　洋子

11.1 Evaluation of Detector Setup

11.1.1 Energy Resolution

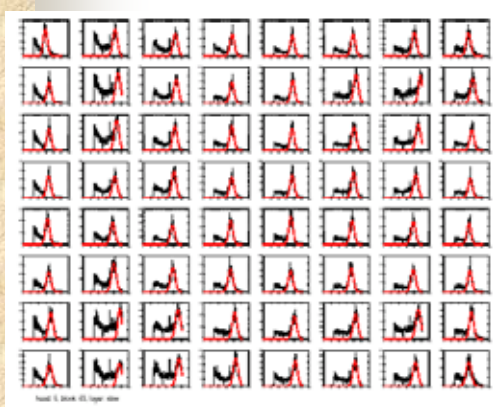

Figure 11.1: Crystal energy spectra of the LSO_{slow} layer from a single detector block. Shown are histograms for each crystal and the gaussian curves fitted to the 511keV energy peaks.

Table 11.1: Mean energy resolution [%] for all detector heads

Head	Crystal Layer			
	LSO_{slow}	LSO_{medium}	LSO_{fast}	GSO
0	20.5	-	29.4	-
1	-	19.5	-	28.0
2	18.8	-	25.8	-
3	-	21.2	-	25.7
4	21.9	-	31.6	-
5	19.5	-	28.5	-
6	20.2	-	26.8	-
7	-	20.5	-	27.3
mean	20.2	20.4	28.4	27.0

- ^{68}Ge line source
- ガウス関数 Fit $G(x) = A_0 \exp^{\frac{-(x-x_0)^2}{2\sigma^2}}$
- 各結晶エネルギー分解能

$$R_{cry} = \frac{2.35\sigma}{x_0}$$

- エネルギー分解能の平均は24%

11.1.1 Energy Resolution

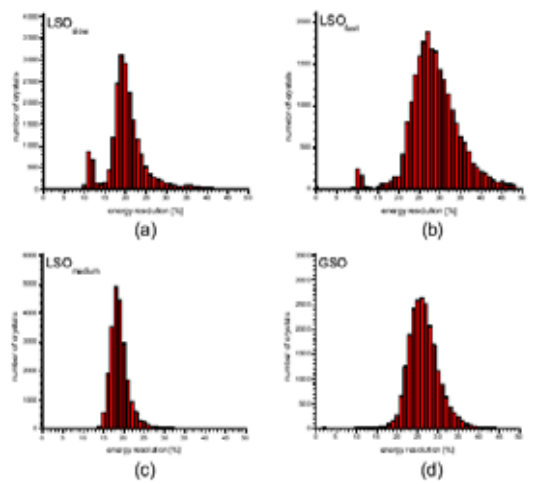

Figure 11.2: Histograms of the measured energy resolution for all crystals of the following layers: (a) LSO_{slow}, (b) LSO_{fast}, (c) LSO_{medium}, (d) GSO .

- LSO_{slow} と LSO_{medium} のエネルギー分解能は平均20%で分散は小さい.
- LSO_{fast} とGSOは分散が大きく分解能も悪い.
  - ← light outputが低いため

11.1.2 Shape Discrimination

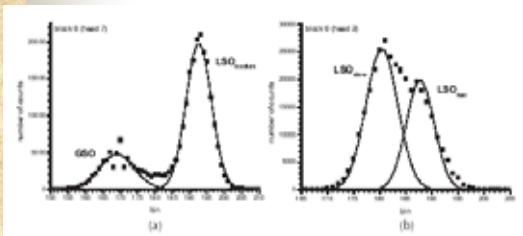

Figure 11.3: Pulse Shape Discrimination. (a) LSO/GSO detector head. (b) LSO/LSO detector head.

Table 11.2: $\overline{R_p}$ [bins] for all detector heads

Head	Crystal Layer			
	LSO_{slow}	LSO_{medium}	LSO_{fast}	GSO
0	184.3	-	193.7	-
1	-	180.8	-	157.1
2	179.0	-	187.1	-
3	-	183.5	-	157.5
4	181.0	-	190.4	-
5	183.3	-	192.1	-
6	178.1	-	185.8	-
7	-	185.2	-	160.1
mean	181.1	183.2	189.8	158.2

- LSO/GSO検出器の2つのピークは容易に弁別できるが、LSO/LSO検出器のピークは接近しており、弁別が難しい.
- LSO_{slow} と LSO_{fast} の平均ピーク位置 R_p の差は 8.7bins 、LSO_{medium} とGSOの差は約3倍の25binsであった.

11.1.2 Shape Discrimination

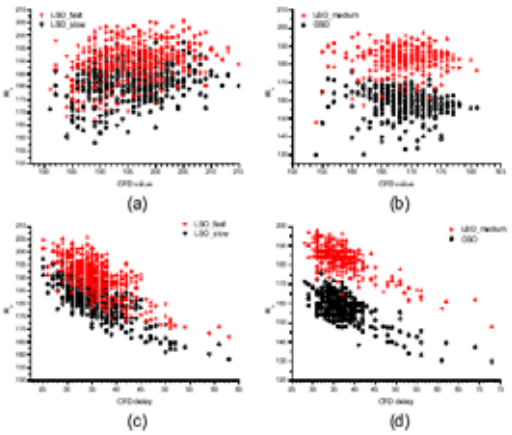

Figure 11.4: $R_p \sim E_1/E_2$ as function of (a) the CFD setting for the LSO/LSO detector blocks, (b) the CFD setting for the LSO/GSO detector blocks, (c) the CFD delay setting for the LSO/LSO detector blocks and (d) the CFD delay setting for the LSO/GSO detector heads.

- RpはCFD値にはほとんど依存しないが、CFD delay値とはexponentialの関係.

↓

time alignmentでCFD delayを調節するとピーク位置が変わるため、shape analysisはtime alignmentの後で行う方がよい.

11.1.3 Time Alignment

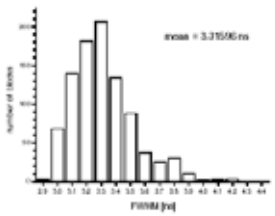

Figure 11.5: Histogram of all timing resolution values from the total number of 936 detector blocks. The mean value of 3.32 ns FWHM reflects the timing resolution of the whole tomograph.

- 全936検出器ブロックの時間分解能のヒストグラムより、平均時間分解能は3.32nsであった.
  - ➔ 6ns wide coincidence windowが可能であり、10nsや12ns timing windowに比べてrandomを減らすことができる.

11.2 Sensitivity

11.2.1 Point Source Measurement

^{22}Na point source

Table 11.3: Sensitivity values [cps/kBq] for point source measurement

Energy Window [keV]	Both Layers	Front Layer	Cross Layer	Back Layer
250-650	70.7	30.2	31.7	10.4
300-650	57.7	24.3	26.4	7.3
350-650	46.5	18.8	21.5	6.3
400-650	37.9	14.9	17.6	5.3
450-650	29.6	11.5	13.9	4.3

- 350-650keVのエネルギーウィンドウではsensitivityは4.7%であった.

11.2.2 Line Source Measurement

$$\varepsilon = \frac{unshielded\ \ trues\ \ count\ \ rate}{activity\ \ within\ \ FOV}$$

$$\varepsilon_{NEMA} = \frac{unshielded\ \ trues\ \ count\ \ rate}{activity\ \ within\ \ line\ \ source}$$

$$N = N_0 \underbrace{B(x, E_\gamma)}_{\text{Buildup factor}} e^{-\mu(x)x}$$

N : attenuation including scatter
N_0: broad beam attenuation

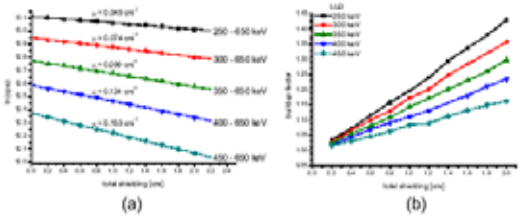

Figure 11.6: (a) Sensitivity measurement with shielded line source. The fit to the data gives the sensitivity of an unshielded source. (b) Buildup factors for this measurement.

Table 11.4: Sensitivity values [cps/kBq] for line source measurement

Energy Window [keV]	ε_{NEMA}	ε			
		both layers	front layer	cross layer	back layer
250-650	9.60	26.9	11.4	12.1	3.3
300-650	8.21	23.0	9.8	10.4	2.8
350-650	6.92	19.4	8.1	8.9	2.5
400-650	5.79	16.2	6.6	7.5	2.2
450-650	4.73	13.2	5.3	6.2	1.8

- μ値は0.049cm^{-1}(250-650keV)、0.153cm^{-1} (450-650keV)であった.
- μ理論値 (0.229cm^{-1} at 511keV)との相違はscattered eventによりカウント数が増えたためと思われる.
- Buildup factorはshieldの増加に伴い増加した.

11.2.2 Line Source Measurement

Table 11.5: μ-values (line source measurement)

Energy Window [keV]	μ-Value [cm^{-1}]	
	uncorrected	scatter corrected
250-650	0.049	0.240
300-650	0.074	0.231
350-650	0.099	0.223
400-650	0.124	0.218
450-650	0.153	0.221

- Scatter補正を行うと、μ値は理論値とほぼ一致した.
- エネルギーウィンドウ450-650keVでは、point sourceと line sourceのsensitivityの比は2.23であった.

Table 11.6: Comparison of sensitivity measurements (ps = point source, ls = line source)

Energy Window [keV]	Sensitivity Ratio (ps/ls)
250-650	2.63
300-650	2.51
350-650	2.40
400-650	2.34
450-650	2.23

11.2.2 Line Source Measurement

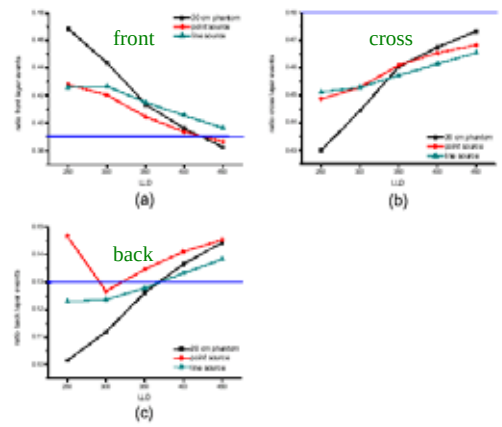

Figure 11.7: (a) Count rate ratio of front layer events, (b) of cross layer events, and (c) of back layer events for three different measurements. The theoretical value is indicated as a straight line.

- 全eventに占めるfront layer、cross layer、back layerのeventの割合は理論値とは異なる.

↓

layer separationが完全ではなく、その精度はエネルギーによって変わる.

11.2.3 3D Sensitivity Profile

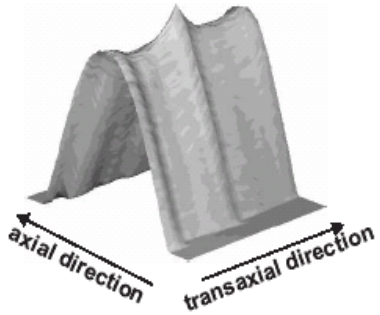

Figure 11.8: 3D sensitivity profile measured with a ^{22}Na point source moved in the axial direction through the FOV. The transaxial direction was scanned in increments of 10mm.

- Sensitivityは中心で最も高い.

11.3 Spatial Resolution (Transaxial Resolution)

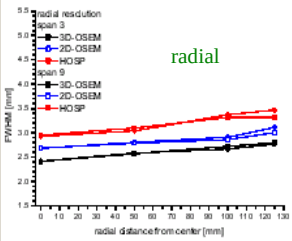

(a)

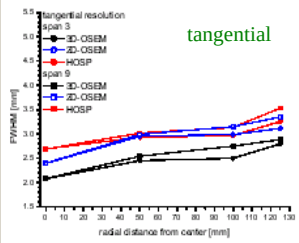

(b)

Figure 11.9

▶span: 3、9

▶reconstruction: 3D-OSEM、FORE+2D-OSEM、FORE+2D-HOSP

- 最もFWHMが良いのはspan3、3D-OSEMの場合の中心で2.42mm (radial)、2.08mm (tangential).
- span3、3D-OSEMの場合、中心から125mmの点でのFWHMは2.77mm (radial)、2.80mm (tangential).
- Radial、tangential resolutionはspanが3と9の場合で変わらない.
- FORE+2D-OSEM、FORE+2D-HOSPでは3D-OSEMに比べて分解能はやや劣るが、span依存性はない.
- HOSPは最も分解能が悪いが、再構成時間は2D-OSEM、3D-OSEMに比べて短い.

11.3 Spatial Resolution (Axial Resolution)

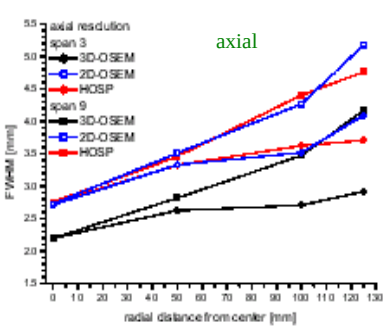

(c)

Figure 11.9

- 中心で2.20mm、125mmで2.92mm (span 3、3D-OSEM)
- 中心で2.73mm、125mmで5.18mm (span 9、2D-OSEM)
- 中心から離れた場所ではspan9、3D-OSEMよりspan3、FORE+2D-HOSPの方が分解能が良い
  - ➔ 分解能劣化はaxial compressionによる

11.3 Spatial Resolution (Volume Resolution)

Volume Resolution = $FWHM_{radial} \cdot FWHM_{tangential} \cdot FWHM_{axial}$

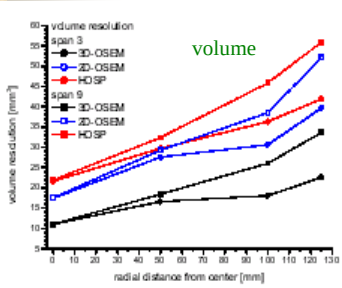

(d)

Figure 11.9: Point source resolution values from different reconstructions with different spans. (a) radial, (b) tangential, (c) axial and (d) corresponding volume resolution for different reconstruction types with different spans.

- Span3、3D-OSEMの場合、FOV200mm以内ではVolume Resolutionは18.1μl以下であった．他のspan、再構成法では、axial resolutionの劣化により、中心から離れるに従って急激にSpatial Resolutionが劣化した．

11.3 Spatial Resolution (Images)

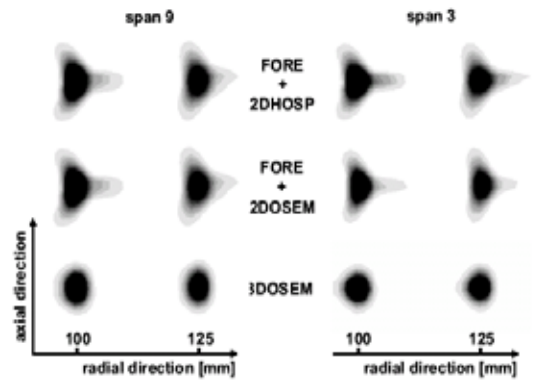

Figure 11.10: Point source images from different reconstruction modes and spans. The maximum color range of all images was set to 10% of the maximum to illustrate the 'foothills' of the images.

- Fore+2Dの場合、axial、radial方向の分解能が劣化.
- 3D-OSEMの場合、span3とspan9でaxial resolutionが異なる.

11.3 Spatial Resolution (Effect of FORE)

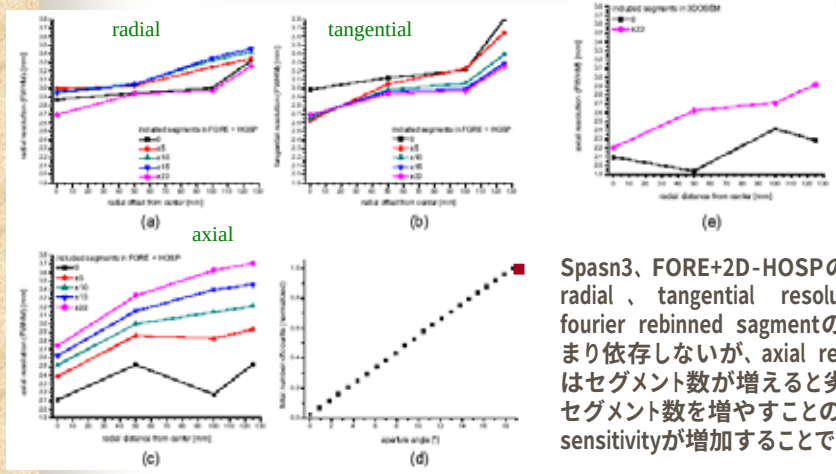

Figure 11.11: Resolution values (span 3) for the point source measurement, reconstructed with different numbers of segments included in FORE. (a) radial, (b) tangential and (c) axial resolution for span 3 + FORE+ HOSP. (d) Integral number of counts for this measurement as a function of the number of included segments. (e) Axial resolution for span 3 + 3D-OSEM.

Spasn3、FORE+2D-HOSPの場合、radial、tangential resolutionはfourier rebinned sagmentの数にあまり依存しないが、axial resolutionはセグメント数が増えると劣化する.セグメント数を増やすことの利点は、sensitivityが増加することである.

Span3、3D-OSEMでは、segmentが0の場合の方が全45segmentの場合よりもaxial resolutionが良い.

11.3 Spatial Resolution (Effect of DOI)

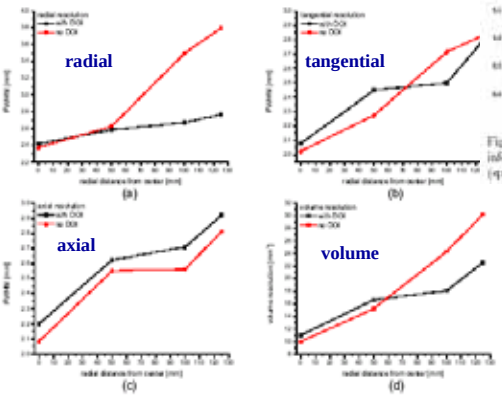

Figure 11.12: Point source measurement with and without DOI information. (a) Radial resolution. (b) Tangential resolution. (c) Axial resolution. (d) Volume resolution.

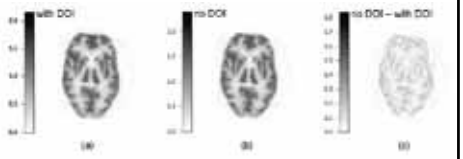

Figure 11.13: Hoffman 3D Phantom measurement. (a) Reconstructed with DOI information (span 3 + 3D-OSEM). (b) Reconstructed without DOI information (span 3 + 3D-OSEM). (c) Difference between images (a) and (b).

- DOIの効果は、radial方向で顕著に現れた.
- Hoffman 3D Phantomでは、DOIを考慮した場合としなかった場合の違いが視覚的には分からない.

11.4 Axial Slice Width

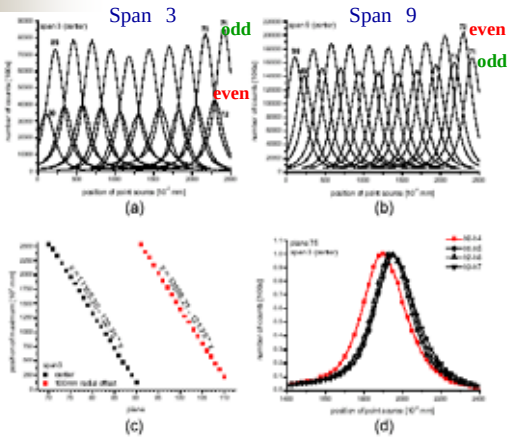

Figure 11.14: Axial slice profiles for planes 71 to 99. (a) Span 3. (b) Span 9. (c) Slice width measured for span 3 in the center and at 100mm radial offset. (d) Normalized slice profiles (plane 75) for specific detector head combinations.

- span3では奇数面、span9では偶数面のsensitivityが高い.
- Maximal count rate の Even/odd は span9 で 1.23 、span3で0.50であった.

Table 11.7: Sensitivity of even and odd planes

	# Planes		Ratio (even/odd)	
	even	odd	theoretical	measured
span 9	5	4	1.25	1.23
span 3	1	2	0.50	0.50

11.4 Axial Slice Width

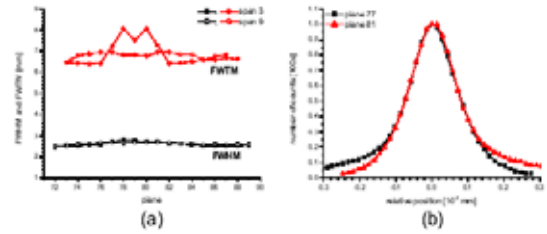

Figure 11.15: (a) FWHM and FWTM for span 3 and span 9 measured in the center. (b) Slice profiles (span 3) for slices 77 and 81 around a block border.

- 中心でのFWHMの平均はspan 3、span 9ともに2.6mm.
- FWTMはspan 9で6.8mm、一方、span 3は面によってばらつきが大きい。

11.5 Scatter

Table 11.8: Scatter fractions (SF) for the NEMA 1994 measurement (ULD 650keV)

LLD [keV]	SF_{air} all layers	SF_{air} front layer	SF_{Water}
250	0.62	0.64	0.69
300	0.58	0.58	0.64
350	0.52	0.53	0.58
400	0.45	0.45	0.51
450	0.35	0.34	0.40

Table 11.9: Scatter fractions (SF) for the improved NEMA 2001 measurement (ULD 650keV)

LLD [keV]	SF NEMA	SF improved NEMA
300	-	0.62
350	0.56	0.56
400	-	0.51
450	-	0.40

- NEMA NU 2-1994 Scatter Phantom
  - エネルギーウィンドウが250-650keVでは62%だったScatter fractionsが450-650keVでは35%に減少した．臨床で使われている350-650keVでは52%であった．
- NEMA NU 2-2001 Scatter Phantom (700mm NEMA Phantom)
  - エネルギーウィンドウ350-650keVでは、scatter fractionは56%であった．
- Improved 700mm NEMA Phantom Measurement
  - 測定値は200mm diameter water phantomとほぼ同じ．